Journal of Fluorine Chemistry 129 (2008) 1110–1113

Contents lists available at ScienceDirect

Journal of Fluorine Chemistry

journal homepage: www.elsevier.com/locate/fluor

Size-dependent upconversion luminescence in YF_3:Yb^{3+}/Tm^{3+} nanobundles

Guofeng Wang, Weiping Qin *, Yue Xu, Lili Wang, Guodong Wei, Peifen Zhu, Ryongjin Kim

State Key Laboratory on Integrated Optoelectronics, College of Electronic Science and Engineering, Jilin University, Changchun 130012, PR China

ARTICLE INFO

Article history:
Received 10 June 2008
Received in revised form 26 July 2008
Accepted 28 July 2008
Available online 19 August 2008

Keywords:
YF_3
Nanobundles
Upconversion luminescence

ABSTRACT

The upconversion luminescent properties of YF_3:Yb^{3+}(20%)/Tm^{3+}(1%) nanobundles with different sizes (240–500 nm in length) were studied under 980-nm excitation. Ultraviolet ($^1I_6 \rightarrow {}^3F_4/{}^3H_6$ and $^1D_2 \rightarrow {}^3H_6$), blue ($^1D_2 \rightarrow {}^3F_4$ and $^1G_4 \rightarrow {}^3H_6$), red ($^1D_2 \rightarrow {}^3H_4$, $^1G_4 \rightarrow {}^3F_4$, and $^3F_3 \rightarrow {}^3H_6$), and near infrared ($^3H_4 \rightarrow {}^3H_6$) emissions were observed. The results indicated that the relative intensity of the ultraviolet to the blue as well as the blue to the near infrared increased with decreasing the size of nanobundles. Especially, the position of the dominant red emission peak varied with the size of nanobundles. As the length of nanobundles increased to 500 nm, unusual $^3F_3 \rightarrow {}^3H_6$ transition was observed, which was theoretically explained considering the decrease of the nonradiative transition rate of $^3F_3 \rightarrow {}^3H_4$.

1. Introduction

Frequency upconversion (UC) from infrared to visible and ultraviolet (UV) by materials doped with trivalent rare-earth (RE) ions has attracted intensive attention for more than 30 years [1]. Recently, great effort has been devoted to the synthesis of nanosized fluorescent materials because the reduction of particle size can result in remarkable modifications of some of their bulk properties [2–6]. Nanosized phosphors or optoelectronic devices usually exhibit novel capabilities, such as tunable luminescence [7], high efficiencies [8], and rapid responsibilities [9], depending on their structure, shape, and size. Taking advantage of these size- and shape-induced changes, infrared to visible/UV UC luminescence in nanocrystals with desired shape and size will play an outstanding role in new optoelectronic devices in the near future [10]. A number of synthesis methods, such as hydrotherm [11], microemulsion [12,13], liquid–solid–solution (LSS) [14], sol–gel [15], and combustion [16], have been developed so far to prepare desired nanostructures.

Among the candidates of UC nanomaterials, fluoride nanocrystals, such as LaF_3, YF_3, and $NaYF_4$, have attracted increasing attention [17–22]. RE-doped fluorides have low phonon energies and high quantum efficiencies as luminescent materials, giving them potential for widespread applications in display devices, short wavelength solid-state lasers, optical communication, and so on [23–25]. Especially, YF_3 nanocrystals, a very important nanofluoride, have been used as host for phosphors with interesting up/down conversion luminescent properties. For example, Li et al. studied the luminescence properties of Ln^{3+}-doped YF_3 nanocrystals [26], Zhang et al. studied the luminescence properties of Ln^{3+}-doped YF_3 nanospindles [27], and Tao et al. investigated the optical properties of truncated octahedral Eu^{3+}-doped YF_3 nanocrystals [28]. Recently, hexagonal and hollow peanut-like YF_3 nanocrystals were synthesized [29,30]. The synthesis and photoluminescence properties of Ln^{3+}-doped YF_3 nanocrystals have become hot topics of nanosized optical functional materials. Despite the fact that some Ln^{3+}-doped YF_3 nanocrystals with special morphologies have been synthesized and some novel spectral phenomena have been observed [24,26,27], shape- and size-dependent UC luminescent behavior of YF_3:Yb^{3+}/Tm^{3+} nanocrystals have received little attention.

In our study, bundled YF_3:Yb^{3+}/Tm^{3+} nanowhiskers were prepared by a facile microemulsion method. The influence of the size of nanowhiskers on UC luminescence was studied systemically. The results indicated that the relative intensity of the ultraviolet to the blue as well as the blue to the near infrared increased with decreasing the size of nanobundles. Besides, the position of the dominant red emission peak varied with the size of nanobundles.

2. Results

2.1. Crystal structure and morphology

The morphology and size of the samples aged for different time were characterized by transmission electron microscope (TEM), as shown in Fig. 1. The average lengths of nanobundles are ~240, ~340, and ~500 nm, for the samples of 24, 48, and 72 h, respectively. The magnified TEM images of an individual nanobundle

* Corresponding author. Tel: +86 431 85168240/8325; fax: +86 431 85168240/8325.
E-mail address: wpqin@jlu.edu.cn (W. Qin).

0022-1139/$ – see front matter © 2008 Elsevier B.V. All rights reserved.
doi:10.1016/j.jfluchem.2008.07.026

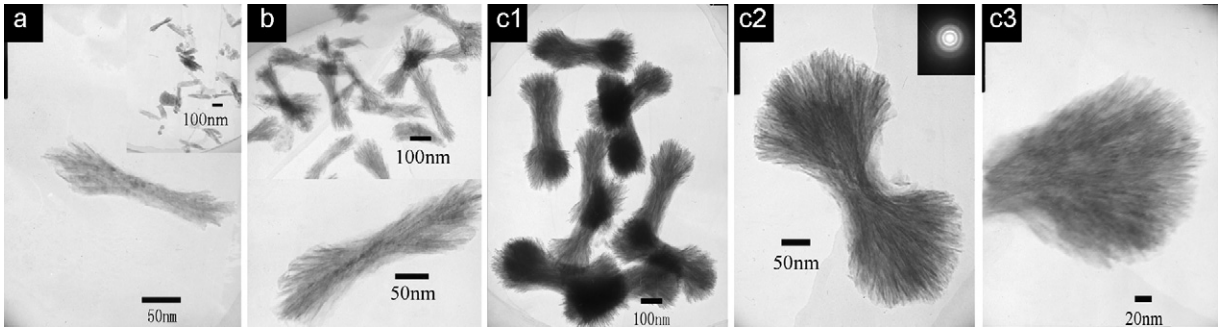

Fig. 1. TEM images of YF_3:Yb^{3+}/Tm^{3+} nanobundles aged for different time: (a) 24 h, (b) 48 h, and (c) 72 h.

(aged for 72 h) indicate that each nanobundle consists of numerous nanowhiskers with a mean diameter of ~2 nm. A typical electron diffraction pattern (inset of Fig. 1c) indicates the polycrystalline structure of YF_3 nanobundles. It is imperative to point out that all of the nanowhiskers are multi-branches. The growth mechanism of nanowhiskers will be discussed in a separate paper in detail. The crystal structure and the phase purity of the samples were obtained by X-ray diffraction (XRD), as shown in Fig. 2. All of the diffraction peaks of the different products can be easily indexed to a pure orthorhombic YF_3 (JCPDS 74-0911). No other impurity peaks were detected. From the bottom to the top in Fig. 2, the widths of the peaks become narrower and narrower (the half width of the diffraction peak (1 1 1) was determined to be 0.742°, 0.539°, and 0.409° for the nanobundles of 24, 48, and 72 h, respectively), suggesting that the crystalline size increases gradually with increasing reaction time.

2.2. UC luminescence from YF_3:Yb^{3+}(20%)/Tm^{3+}(1%) nanobundles with different sizes

As mentioned above, the size and morphology of YF_3:Yb^{3+}/Tm^{3+} nanocrystals would have greatly influence on their UC luminescence properties [7]. Fig. 3(I) shows the normalized UC luminescence spectra of different YF_3:Yb^{3+}(20%)/Tm^{3+}(1%) nanobundles (240–500 nm in length) under 980-nm excitation (180 W/cm^2). The near infrared, red, blue, and UV emissions were observed. The emissions come from the following transitions: $^1I_6 \rightarrow {}^3H_6$ (~291 nm), $^1I_6 \rightarrow {}^3F_4$ (~347 nm), $^1D_2 \rightarrow {}^3H_6$ (~363 nm), $^1D_2 \rightarrow {}^3F_4$ (~454 nm), $^1G_4 \rightarrow {}^3H_6$ (~475 nm), $^1D_2 \rightarrow {}^3H_4$ (~643 nm), $^1G_4 \rightarrow {}^3F_4$ (~649 nm), $^3F_3 \rightarrow {}^3H_6$ (~687 nm), and $^3H_4 \rightarrow {}^3H_6$ (~790 nm). Fig. 3(II) shows the magnification of the spectra in the range of 600–750 nm. It is surprising to observe that the red emission band centered at 643 nm ($^1D_2 \rightarrow {}^3H_4$), 649 nm ($^1G_4 \rightarrow {}^3F_4$), and 687 nm ($^3F_3 \rightarrow {}^3H_6$), for the samples of 240, 340, and 500 nm respectively.

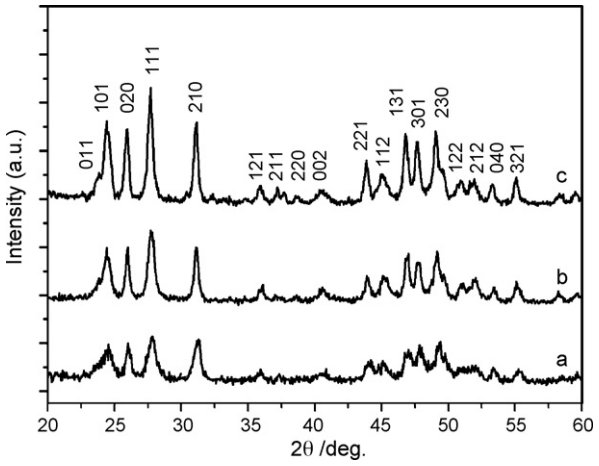

Fig. 2. XRD patterns of YF_3:Yb^{3+}/Tm^{3+} nanobundles aged for different time: (a) 24 h, (b) 48 h, and (c) 72 h.

Fig. 3(III) shows the spectra of different samples in the range of 730–850 nm. When the mean length of nanowhiskers was 240 nm, two shoulders appeared in the short wavelength side of the main peak located at ~790 nm ($^3H_4 \rightarrow {}^3H_6$), which correspond to $^1D_2 \rightarrow {}^3F_3$ and $^1D_2 \rightarrow {}^3F_2$ transitions, respectively [31]. With increasing the size of nanowhiskers, the shoulders became illegible. Furthermore, the relative intensity of the ultraviolet to the blue as well as the blue to the near infrared increased with decreasing the size of nanowhiskers, which will be discussed in Section 3.

2.3. Power-dependence of UC luminescence

Fig. 4 shows the intensity ratio (σ) of $^1G_4 \rightarrow {}^3H_6$ to $^3H_4 \rightarrow {}^3H_6$ as a function of excitation power in 500-nm nanobundles. We can see that σ increased with the increase of excitation power, which can be explained by the expanded study of rate equation [32]. Let γ represent the radiative transition rate of $^3H_4 \rightarrow {}^3H_6$, N_0 and N the population of the states $^2F_{7/2}$ (Yb^{3+}) and $^3H_4$ (Tm^{3+}), X the rate of energy transfer (ET) $^2F_{5/2} \rightarrow {}^2F_{7/2}$:$^3H_4 \rightarrow {}^1G_4$, F the pump power, and Ω the absorption cross-section of Yb^{3+}. According to the steady-state rate equation [32], we have [33]

$$\sigma \propto \frac{NN_0XF\Omega}{\gamma}$$

therefore, the fluorescence ratio (σ) should enhance with the increase of excitation power. However, σ did not change linearly against excitation power. Presumably, two mechanisms might cause the nonlinear change of σ. (1) As shown in Fig. 3, the $^3H_4 \rightarrow {}^3H_6$ overlapped with the $^1D_2 \rightarrow {}^3F_3/{}^3F_2$, which increased with increasing excitation power. Then the integrated area of the emission band $^3H_4 \rightarrow {}^3H_6$ should be larger than its actual area owing to the $^1D_2 \rightarrow {}^3F_3/{}^3F_2$. Here, the intensity ratio was the integrated area ratio of the two emission bands ($^1G_4 \rightarrow {}^3H_6$ and $^3H_4 \rightarrow {}^3H_6$). Consequently, the intensity ratio nonlinearly changed against excitation power. (2) The nonlinear change might be attributed to saturation and thermal effects [7], which could result in the decrease of the emission intensities of the $^1G_4 \rightarrow {}^3H_6$ and $^3H_4 \rightarrow {}^3H_6$.

3. Discussion

3.1. Population and photoluminescence processes

Fig. 5 shows the UC luminescence mechanism and population processes in Yb^{3+}/Tm^{3+}-codoped systems. According to our previous report [33], the population of the states $^1I_6$, $^1D_2$, $^1G_4$,

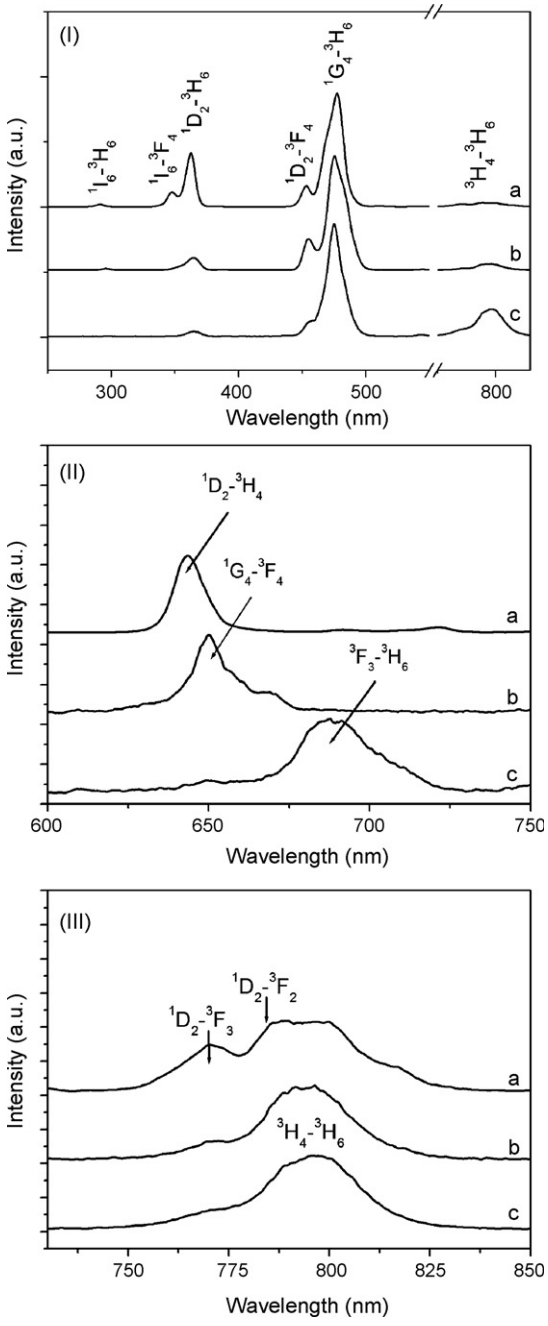

Fig. 3. UC luminescence spectra of YF_3:Yb^{3+}(20%)/Tm^{3+}(1%) nanobundles aged for different time under 980-nm excitation (180 W/cm^2): (a) 24 h, (b) 48 h, and (c) 72 h.

and $^3H_4$($^3F_3$) come from five-photon, four-photon, three-photon, and two-photon UC processes, respectively. The 980-nm diode laser is only completely resonant with $^2F_{7/2} \rightarrow {}^2F_{5/2}$ absorption of Yb^{3+} at 980 nm but not resonant with the ground absorption of Tm^{3+} at all.

The near infrared UC luminescence occurs via a two-step ET from Yb^{3+} to Tm^{3+}. First, the Tm^{3+} ions are excited from the ground-state $^3H_6$ to the excited-state $^3H_5$ via ET of neighboring Yb^{3+} and Tm^{3+}. Subsequent nonradiative relaxation of $^3H_5 \rightarrow {}^3F_4$ populates the $^3F_4$ level. In the second-step excitation, the same laser pumps the excited-state atoms from the $^3F_4$ to the $^3F_2$ state via ET. The populated $^3F_2$ may nonradiatively relax to two levels: $^3F_3$ and $^3H_4$, which produce red (~687 nm) and near infrared (~790 nm) emissions [33], respectively. The electrons in the $^3H_4$ level may

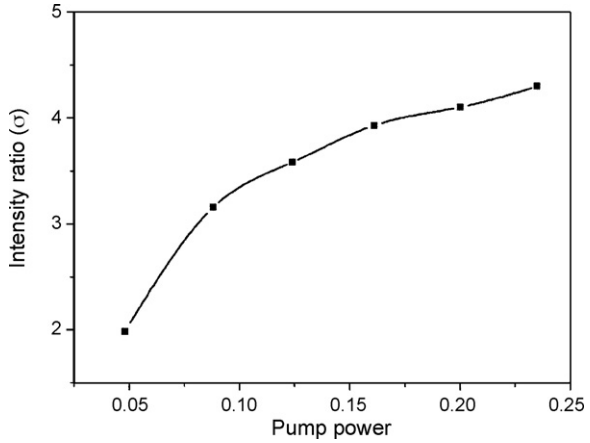

Fig. 4. Intensity ratio (σ) of the $^1G_4 \rightarrow {}^3H_6$ to the $^3H_4 \rightarrow {}^3H_6$ as a function of excitation power in YF_3:Yb^{3+}(20%)/Tm^{3+}(1%) nanobundles aged for 72 h.

be partly excited to the $^1G_4$ level via phonon-assisted ET by the third photon, produce blue (475 nm) and red (649 nm) emissions simultaneously. Owing to the very small energy gap of ~580 cm^{-1} between $^3F_2$ and $^3F_3$, no luminescence from the $^3F_2$ state can be found.

The $^1D_2$ level of Tm^{3+} cannot be populated by the fourth photon from Yb^{3+} to the $^1G_4$ level via ET due to the large energy mismatch (about 3500 cm^{-1}) between them. The cross relaxation process of $^3F_2 + {}^3H_4 \rightarrow {}^3H_6 + {}^1D_2$ between Tm^{3+} ions may alternatively play an important role in populating $^1D_2$ level. The populated $^1D_2$ level relaxes radiatively to the ground-state and inter-states, which cause 363-, 454-, and 643-nm emissions. On the other hand, the electron in the $^1D_2$ level may be excited to the $^1I_6$ level via another ET process, produce 291- and 347-nm emissions, simultaneously.

3.2. The effect of nonradiative transition of $^3F_3 \rightarrow {}^3H_4$ on UC luminescence

For the $^3H_4 \rightarrow {}^3H_6$ emission, the nonradiative transition of $^3F_3 \rightarrow {}^3H_4$ is involved. The nonradiative transition of $^3F_3 \rightarrow {}^3H_4$ competes with the radiative transition of $^3F_3 \rightarrow {}^3H_6$. In most case,

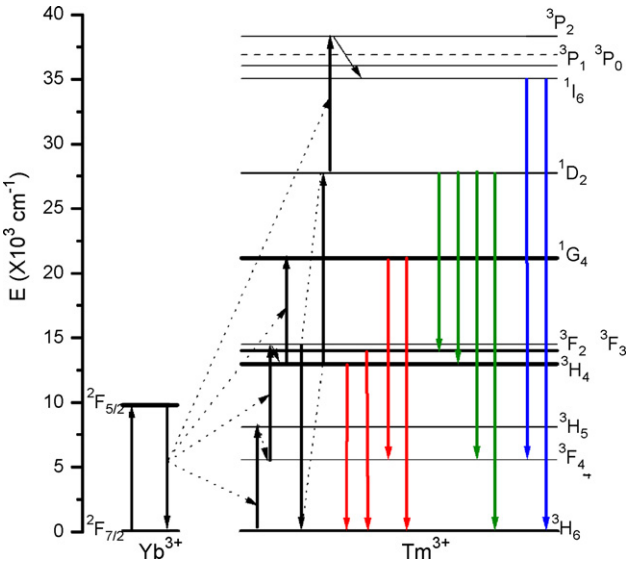

Fig. 5. UC mechanism of Yb^{3+}-sensitized Tm^{3+} emissions in YF_3:Yb^{3+}(20%)/Tm^{3+}(1%) nanobundles.

the $^3F_3 \rightarrow {}^3H_6$ emission is hardly observed due to the fast nonradiative transition of $^3F_3 \rightarrow {}^3H_4$ [34]. However, the crystallinity of product is improved with increasing aging time, which helps to decrease nonradiative transition rate. Therefore, the $^3F_3 \rightarrow {}^3H_4$ would decrease with increasing aging time. When the aging time increased to 72 h, the $^3F_3 \rightarrow {}^3H_6$ emission was observed (Fig. 3). Subsequently, the reduced population of $^3H_4$ level may lead the ET of $^3H_4$ (Tm^{3+}) + $^2F_{5/2}$ (Yb^{3+}) → $^1G_4$ (Tm^{3+}) + $^2F_{3/2}$ (Yb^{3+}) and the cross relaxation of $^3F_2 + {}^3H_4 \rightarrow {}^3H_6 + {}^1D_2$ to decrease, resulting in the decreased populations of $^1G_4$ and $^1D_2$. Furthermore, our previous results indicated that the intensity ratio (σ) of $^1G_4 \rightarrow {}^3H_6$ to $^3H_4 \rightarrow {}^3H_6$ was proportional to the population of the $^3H_4$ [33]. Therefore, σ would decrease with increasing aging time. On the contrary, the populations of $^1G_4$ and $^1D_2$ level increased with decreasing aging time, which resulted in the appearance of the transitions of $^1G_4 \rightarrow {}^3F_4$ and $^1D_2 \rightarrow {}^3H_4$ instead of $^3F_3 \rightarrow {}^3H_6$.

4. Conclusions

In summary, the upconversion luminescent properties of YF_3:Yb^{3+}(20%)/Tm^{3+}(1%) nanobundles with different sizes were studied systemically. The size of nanowhiskers could be well controlled by changing aging time. Under 980-nm excitation, ultraviolet ($^1I_6 \rightarrow {}^3F_4/{}^3H_6$ and $^1D_2 \rightarrow {}^3H_6$), blue ($^1D_2 \rightarrow {}^3F_4$ and $^1G_4 \rightarrow {}^3H_6$), red ($^1D_2 \rightarrow {}^3H_4$, $^1G_4 \rightarrow {}^3F_4$, and $^3F_3 \rightarrow {}^3H_6$), and near infrared ($^3H_4 \rightarrow {}^3H_6$) emissions were observed. The results indicated that the relative intensity of the ultraviolet to the blue as well as the blue to the near infrared increased with decreasing the size of nanowhiskers. Besides, the red emission band centered at 643 nm ($^1D_2 \rightarrow {}^3H_4$), 649 nm ($^1G_4 \rightarrow {}^3F_4$), and 687 nm ($^3F_3 \rightarrow {}^3H_6$), for the samples of 240, 340, and 500 nm respectively.

5. Experimental

5.1. Samples preparation

Y_2O_3, Yb_2O_3, and Tm_2O_3 (purity ≥ 99.99%) were supplied by Shanghai Chemical Reagent Company. Cetyltrimethylammonium bromide (CTAB), cyclohexane, 1-pentanol, NaF, and HCl were supplied by Beijing Chemical Reagent Company, and were of analytical grade. All the reagents and solvents were used as received without further purification. Distilled water was used to prepare solutions. Ln_2O_3 (Ln = Y, Yb, and Tm) were completely dissolved in dilute HCl by heating to prepare the stock solution of $LnCl_3$.

Two identical solutions, denoted as microemulsion I and II, were prepared by dissolving 2.25 g of CTAB in 50 mL of cyclohexane and 2.5 mL of 1-pentanol. The two microemulsions were stirred separately for 30 min, and then 2 mL of 0.5 M $LnCl_3$ (Ln = Y, Yb, and Tm) aqueous solution and 2 mL of NaF aqueous solution were added dropwise to microemulsion I and II, respectively. After vigorous stirring, the two optically transparent microemulsion solutions were mixed. After aging for 72 h, the emulsion mixture was centrifuged at 12,000 rpm for 10 min, which caused sedimentation of the product and allowed removal of mother liquor. The product was then washed with distilled water and absolute ethanol in turn, and finally dried in vacuum at 80 °C for 4 h. To improve the crystallinity of the nanocrystalline powders, all of the resultant products were annealed at 450 °C.

5.2. Measurements and characterization

Phase identification was performed via X-ray powder diffractometer (XRD, Rigaku RU-200b) using a nickel-filtered Cu Kα radiation (λ = 1.4518 Å) in the range of $20^\circ \leq 2\theta \leq 60^\circ$. The size and morphology were characterized by transmission electron microscope (TEM, JEM 2010 with operating voltage of 200 kV). TEM samples were prepared by ultrasonic nebulization of ethanolic dispersion on a lacey-film copper grid.

The UC luminescence spectra were recorded with a Hitachi F-4500 fluorescence spectrophotometer under 980-nm excitation. For comparison of the UC luminescence properties of different samples, the luminescence spectra were measured with the same instrument parameters (2.5 nm for slit width and 400 V for PMT voltage). All the experiments were performed at room temperature.

Acknowledgment

This research was supported by Natural Science Foundation of China (Grant Nos. 10474096 and 50672030).

References

[1] T. Kano, H. Yamamoto, Y. Otomo, J. Electrochem. Soc. 119 (1972) 1561–1564.
[2] B. Tissue, Chem. Mater. 10 (1998) 2837–2845.
[3] Y. Soo, S. Huan, Y. Kao, V. Chabra, B. Kulkarni, J. Veliadis, R. Bhargava, Appl. Phys. Lett. 75 (1999) 2464–2466.
[4] M. Yin, C. Duan, W. Zhang, L. Lous, S. Xia, J. Krupa, J. Appl. Phys. 86 (1999) 3751–3757.
[5] G. Hebbink, J. Stouwdam, D. Reinhoudt, F. vanVeggel, Adv. Mater. 14 (2002) 1147–1150.
[6] A. Huignard, V. Buissette, A. Franville, T. Gacoin, J. Boilot, J. Phys. Chem. B 107 (2003) 6754–6759.
[7] X. Bai, H. Song, G. Pan, Y. Lei, T. Wang, X. Ren, S. Lu, B. Dong, Q. Dai, L. Fan, J. Phys. Chem. C 111 (2007) 13611–13617.
[8] R. Bhargava, D. Gallaghar, X. Hong, A. Nurmikko, Phys. Rev. Lett. 72 (1994) 416–419.
[9] Y. Kim, Y. Yang, S. Ha, S. Cho, Y. Kim, H. Kim, H. Yang, Y. Kim, Sens. Actuators B 106 (2005) 189–198.
[10] K. Kawano, K. Arai, H. Yamada, N. Hashimoto, R. Nakata, Sol. Energy Mater. Sol. Cells 48 (1997) 35–41.
[11] X. Wang, Y. Li, Chem. Eur. J. 9 (2003) 5627–5635.
[12] M. Cao, Y. Wang, Y. Qi, C. Guo, C. Hu, J. Solid State Chem. 177 (2004) 2205–2209.
[13] M. Schwuger, K. Stickdom, R. Schomacker, Chem. Rev. 95 (1995) 849–864.
[14] L. Wang, Y. Li, Chem. Mater. 19 (2007) 727–734.
[15] A. Patra, C. Friend, R. Kapoor, N. Prasad, J. Phys. Chem. B 106 (2002) 1909–1912.
[16] Y. Tao, G. Zhao, W. Zhang, S. Xia, Mater. Res. Bull. 32 (1997) 501–506.
[17] S. Sivakumar, F. Veggel, P. May, J. Am. Chem. Soc. 129 (2007) 620–625.
[18] Y. Wang, W. Qin, J. Zhang, C. Cao, J. Zhang, Y. Jin, P. Zhu, G. Wei, G. Wang, L. Wang, Chem. Lett. 36 (2007) 1–3.
[19] X. Wang, J. Zhuang, Q. Peng, Y. Li, Inorg. Chem. 45 (2006) 6661–6665.
[20] C. Li, Z. Quan, P. Yang, J. Yang, H. Lian, J. Lin, J. Mater. Chem. 18 (2008) 1353–1361.
[21] C. Li, J. Yang, Z. Quan, P. Yang, D. Kong, J. Lin, Chem. Mater. 19 (2007) 4933–4942.
[22] C. Li, Z. Quan, J. Yang, P. Yang, J. Lin, Inorg. Chem. 46 (2007) 6327–6329.
[23] G. De, W. Qin, J. Zhang, J. Zhang, Y. Wang, C. Cao, Y. Cui, J. Solid State Chem. 179 (2006) 955–958.
[24] J. Zhang, W. Qin, J. Zhang, Y. Wang, C. Cao, Y. Jin, G. Wei, G. Wang, L. Wang, J. Nanosci. Nanotechnol. 8 (2007) 1–4.
[25] C. Cao, W. Qin, J. Zhang, Y. Wang, P. Zhu, G. Wei, G. Wang, R. Kim, L. Wang, Opt. Lett. 33 (2008) 857–859.
[26] R. Yan, Y. Li, Adv. Funct. Mater. 15 (2005) 763–770.
[27] M. Zhang, H. Fan, B. Xi, X. Wang, C. Dong, Y. Qian, J. Phys. Chem. C 111 (2007) 6652–6657.
[28] F. Tao, Z. Wang, L. Yao, W. Cai, X. Li, J. Phys. Chem. C 111 (2007) 3241–3245.
[29] J. Lemyre, A. Ritcey, Chem. Mater. 17 (2005) 3040–3043.
[30] M. Wang, Q. Huang, H. Zhang, X. Chen, Z. Xue, X. You, Cryst. Growth Des. 10 (2007) 2106–2111.
[31] M. Noginov, M. Curley, P. Venkateswarlu, A. Williams, J. Opt. Soc. Am. B 14 (1997) 2126–2136.
[32] S. Huang, S. Lai, L. Lou, W. Jia, W. Yen, Phys. Rev. B 24 (1981) 59–63.
[33] G. Qin, W. Qin, C. Wu, S. Huang, D. Zhao, J. Zhang, S. Lu, Solid State Commun. 125 (2003) 377–379.
[34] T. Riedener, H. Güdel, G. Valley, R. McFarlane, J. Lumin. 63 (1995) 327–337.